Title: Post-processing strategies in Image Scanning Microscopy

Author names and affiliations:

McGregor, J. E.[a, 1], Mitchell, C. A.[a, 1], Hartell, N.A.[a, *]

[a] Department of Cell Physiology and Pharmacology, University of Leicester, University Road, Leicester, UK, LE1 7RH

[1] These authors contributed equally to this work.

* Corresponding author, postal address: Department of Cell Physiology and Pharmacology, University of Leicester, University Road, Leicester, UK, LE1 7RH, phone: +441162523301, fax: +44116 252 5045, email: nh88@leicester.ac.uk

Abstract

Image scanning microscopy (ISM) coupled with pixel reassignment offers a resolution improvement of 1.41 over standard widefield imaging. By scanning point-wise across the specimen and capturing an image of the fluorescent signal generated at each scan position, additional information about specimen structure is recorded and the highest accessible spatial frequency is doubled. Pixel reassignment can be achieved optically in real time or computationally *a posteriori* and is frequently combined with the use of a physical or digital pinhole to reject out of focus light. Here, we simulate an ISM dataset using a test image and apply standard and non-standard processing methods to address problems typically encountered in computational pixel reassignment and pinholing. We demonstrate that the predicted improvement in resolution is achieved by applying standard pixel reassignment to a simulated dataset and explore the effect of realistic displacements between the reference and true excitation positions. By identifying the position of the detected fluorescence maximum using localisation software and centring the digital pinhole on this co-ordinate before scaling around translated excitation positions, we can recover signal that would otherwise be degraded by the use of a pinhole aligned to an inaccurate excitation reference. This strategy is demonstrated using experimental data from a multiphoton ISM instrument. Finally we investigate the effect that imaging through tissue has on the positions of excitation foci at depth and observe a global scaling with respect to the applied reference grid. Using simulated and experimental data we explore the impact of a globally scaled reference on the ISM image and by pinholing around the detected maxima, recover the signal across the whole field of view.

Keywords (max. 6): Optical microscopy, Super-resolution, Pixel reassignment, Point spread function, Pinhole, Image formation

1. Introduction

'Image scanning microscopy' (ISM) differs from conventional scanning microscopy techniques in that an image of the emission produced by each excitation focus is recorded rather than a single value from a photo multiplier tube. This approach offers an improved signal to noise ratio and increased resolution with relatively little modification to the existing hardware of a laser-scanning microscope. There are now several different implementations of ISM, underpinned by the concept of 'pixel reassignment' [1-3], achieved either by optical (ISIM [4, 5], OPRA [6]) or computational means (MSIM [7] & spinning disk ISM [8]. This manuscript will explore the potential of computational approaches utilizing methods drawn from single molecule localization microscopy for *a posteriori* pixel reassignment.

To understand the concept of pixel reassignment, it is helpful to consider a single image of the fluorescence generated by a single excitation focus. Each pixel on the camera can be considered as a 'micropinhole' [4], displaced by some distance from the excitation axis. Like a pinhole camera, each pixel 'micropinhole' detects an image of the emitted fluorescence; the smaller the pinhole, the sharper the image. It is these multiple copies of the signal, each detected by a single, point-like pixel acting as a stopped down confocal pinhole,

which underlies the improved resolution offered by this approach. If each displaced copy of the image can be correctly overlaid, the fluorescent image formed by a single excitation focus will become sharper and higher intensity. The images of all the excitation foci are then summed together to form a complete image of the specimen with enhanced resolution.

Figure 1 illustrates the principle of pixel reassignment in terms of excitation and detection point spread functions. The further a pixel is from an excitation source, the dimmer the intensity of the image it detects, although the resolution is not degraded [7, 9]. This is because the probability of detecting a photon at the displaced pixel depends on the overlap (multiplication) between the detection point spread function (PSF_{det}) and the excitation point spread function (PSF_{ex}). PSF_{det} is centred on the detection axis and characterises the probability of a photon being collected by that pixel. PSF_{em} is centred on the excitation axis and characterises the probability of a photon being emitted. To detect a fluorescent signal, both excitation and detection are required so the probability distributions are multiplied; the result of this multiplication is the 'effective' PSF (PSF_{eff}) of the imaging system. The further apart these PSFs are, the smaller the overlap and the lower the probability of detecting a signal. This results in a lower intensity image. However there is also a spatial consequence of imaging with a displaced pinhole. Assuming that both emission and excitation point spread functions are identical, as would be the case for single photon fluorescence with no Stokes shift, the probability of an excitation and detection event is maximal at the position midway between the excitation and detection maxima. Because the detected light is therefore most likely to have originated from this position, it can be 'reassigned' to a location half the original distance from the excitation focus [1, 6, 8]. Performing this for each pixel corresponds to scaling the image by a factor of ½ around the excitation focus. In general the excitation and emission wavelengths are different, resulting in excitation and detection PSFs of different widths, meaning that the position of the maximum of the resulting multiplication, and therefore the appropriate scaling factor (m), is slightly larger than ½ [6]. Approximating the PSFs as Gaussian, the appropriate theoretical scaling factor is given by equation 1 [6]. In practice, a factor of ½ is used [see 5, 6, 8].

$$m = \frac{{\sigma_{ex}}^2}{{\sigma_{ex}}^2 + {\sigma_{em}}^2} \qquad [1]$$

Before scaling, the image generated by each excitation focus may be multiplied by a Gaussian function to simulate a 'macropinhole' [7]. This process provides axial sectioning, removing out of focus light by mimicking the effect of a confocal pinhole. Additionally, it suppresses background noise and pixel cross-talk between neighbouring excitation foci in a single exposure. The final image is the sum of the images generated at each excitation focus as the laser scans across the specimen. The width of the effective PSF can also be calculated using the standard deviations of the emission and excitation PSFs using equation 2 [6]; this value defines the resolution of the final ISM image and can be used to inform any subsequent deconvolution. The processes involved in ISM are summarised in figure 2.

$${\sigma_{eff}}^2 = m^2 {\sigma_{em}}^2 + (m-1)^2 \, {\sigma_{ex}}^2 \qquad [2]$$

It is possible to scale each image around the excitation focus optically by descanning the emitted light and demagnifying the image of each excitation focus [4, 6] or doubling the spacing between excitation foci [5, 10]. This has the advantage of performing the scaling step in real time rather than at the post-processing stage. Unfortunately not all microscopes are amenable to this fully optical approach. Acousto-optic devices, used in random access microscopes, have wavelength-dependent and inefficient transmission characteristics making it impractical to use the same scanning device for descanning. In such cases it is necessary to have a separate method of identifying the positions of the excitation foci in order to scale around them. However, the position of the detected fluorescence emission maximum will only reveal the exact location of the excitation focus in uniformly fluorescent specimens. This is because the detected emission is the result of PSF_{ex} multiplied by the

fluorophore distribution in the specimen and then convolved with PSF_{det} (figure 3A). Consequently a uniformly fluorescing sample, such as a thin layer of fluorescein solution, is typically used as a reference to determine the positions of the excitation foci [7, 8].

In practice, the excitation pattern may change between imaging the reference and imaging the specimen due to changes in focal plane, refractive index of the specimen, or mechanical drift. If the specimen is illuminated with a known, periodic excitation pattern it is possible to infer the positions of the excitation foci from the detected emission maxima using Fourier methods [7, 11]. However this approach breaks down if the specimen itself has a periodic structure, or if the specimen is sparsely labelled, for example in the case of imaging punctate biological structures or sub-resolution beads. Similarly, sparse excitation patterns, as may be employed in high speed imaging of a reduced field of view, would also pose a potential problem for this method.

In this paper we use both synthetic and experimental data to explore how inaccurate identification of the position of excitation foci affects the resulting image. We examine whether a combination of scaling around excitation foci and pinholing around the detected emission maxima may offer a practical solution to image degradation caused by the use of a translated excitation reference. If ISM is used to image at depth through tissue, the refractive index profile of the specimen may lead to the global displacement of the true excitation foci relative to the applied excitation pattern. We investigate the effect of imaging at depth on the positions of excitation foci and assess the impact of processing data with a globally scaled excitation reference. Additionally, we examine the possibility of scaling around the emission maxima (figure 3B) as an interim processing step in situations where the where the true excitation pattern is unknown or yet to be determined.

2. Materials and methods

2.1 Synthetic data

Simulated ISM data were generated using code written in MATLAB (MATLAB and Image Processing Toolbox Release 2014a, The MathWorks, Inc., MA, USA). A 400 x 400 pixel image of fluorescent actin stress fibres within a fibroblast cell (Catherine Nobes and Alan Hall, Wellcome Images, London, UK) was used as the test image. 2D Gaussian excitation and detection PSFs were constructed based on theoretical, diffraction-limited FWHM [12, 13], assuming a pixel size of 57.4 nm and wavelengths of 488 and 515 nm respectively. The pixel size used was consistent with that of a typical ISM microscope to accurately simulate the size and displacements of the PSFs but the test image pixel size is arbitrary and any measurements made from the image do not therefore correspond to expected physical sizes. The data generation process is illustrated in figure 4. A square array of 18 x 18 excitation PSFs was constructed and the image was multiplied by this excitation array. The resulting product was convolved with the detection PSF to simulate the signal collected in the image plane. The excitation array was then raster scanned across the test image one pixel at a time and the process repeated at each point (21 x 21 points in total). A stack of 441 images was ultimately created to mimic a data stack collected during an ISM scan along with a list of excitation coordinates for each frame in the stack.

2.2 Experimental data

Example ISM datasets used a 16 by 16 array of excitation foci stepped 21 by 21 times and the subsequent emitted fluorescence images were collected onto a 512 x 512 pixel array. Images of autofluorescent pollen (Carolina Biological Supply Company, Burlington, VT, USA) and immunostained alpha-tubulin in cultured SH-SY-5Y neuroblastoma cells were collected using an upright multiphoton ISM system equipped with a 60x water-dipping objective (NA 1.0; Nikon, Tokyo, Japan). Acousto-optic devices (Isomet, Springfield, VA, USA) were used for high-speed laser positioning in x and y dimensions and images were collected with an sCMOS camera (Neo; Andor Technology, Belfast, UK). SH-SY-5Ys cells were cultured in DMEM supplemented with 10 % foetal calf serum and antibiotic (Penicillin Streptomycin 100 Uml-1; All Life Technologies, Carlsbad, CA, USA). Cells were passaged twice weekly at a 1 in 3 ratio. Two days prior to fixing, cells were seeded onto no. 1.5 glass

coverslips in 24-well plates (Thermo Fisher Scientific, Waltham, MA, USA) and allowed to adhere. To fix the cells, the medium was aspirated and cells were incubated with 4 % paraformaldehyde in phosphate buffered saline (PBS; Life Technologies) for 20 minutes at room temperature. Cells were then washed in PBS before membrane permeabilisation using 0.2 % Triton X-100 (Sigma-Aldrich. St. Louis, M, USA) and 1 % BSA in PBS. After washing with PBS, cells were incubated for 1 hour at room temperature with a 1:200 dilution of a monoclonal mouse α-tubulin antibody (Sigma-Aldrich) in 1 % BSA. The antibody was aspirated and the cells were washed in PBS before the addition of the 1:200 dilution in 1 % BSA of a secondary antibody (goat anti-mouse Alexa546; Life Technologies). Finally, cells were washed in PBS before coverslips were mounted in ProLong Gold (Life Technologies) on glass microscope slides.

2.3 Reference grid displacement measurements

Uniformly fluorescent reference slides were prepared with either fluorescein (Sigma-Aldrich, St. Louis. MO, USA) in water or fluorescein in mowiol (Calbiochem, Billerica, MA, USA) sandwiched between a glass slide and coverslip. A plastic fluorescent slide was also used (Chroma Technology Corp., Bellows Falls, VT, USA). Reference image excitation grids were created by performing ISM scans across uniform fluorescent reference slides. An acousto-optic device (Isomet) was used to generate excitation grid patterns in x and y dimensions at high speed. For single photon measurements, a 488 nm argon-ion laser was used for excitation (Modu-Laser, West Jordan, UT, USA) and images were collected with a CCD camera (Orca; Hamamatsu, Hamamatsu, Japan). Reference scans were taken at three different locations on each type of reference slide with a 5-hour time delay to assess system drift under realistic experimental conditions. The lateral displacement between difference reference scans was determined by image registration performed in Igor Pro and the mean and standard deviation of the absolute displacements were determined. Angular displacement and skew were negligible.

To assess the effect of imaging at depth, positions of excitation foci in a brightly fluorescent plastic slide (Chroma Technology Corp) were determined in the presence and absence of a 200 µm slice of fixed mouse brain tissue placed on the surface of the slide above the focal plane. Animals less than 3 months of age were culled in accordance with Home Office regulations and the brains quickly removed and placed in an ice cold artificial cerebrospinal fluid (aCSF) consisting of (in mM); 127 NaCl; 1.25 KH_2PO_4; 1.30 $MgSO_4.7H_2O$); 26 $NaHCO_3$; 1.61 KCl; 10 glucose (all Sigma-Aldrich), equilibrated with 95% O2–5% CO_2 to pH 7.4. Transverse hippocampal slices, 200 µm thick, were prepared using a vibratome (DSK-1000; Dosaka, Kyoto, Japan) and equilibrated at room temperature in the same solution for at least one hour. Slices were fixed in 4 % paraformaldehyde in PBS overnight. The fixation buffer was aspirated and the slices were washed four times in PBS before being immersed in PBS for storage. Fixed slices were kept at $4^{o}C$ until required. ACSF was pipetted onto the tissue and used as the objective immersion medium. The multiphoton system outlined in section 2.2 was used to apply an excitation grid pattern at the top of the fluorescent slide with and without brain tissue present, as well as in standard fluorescein and mowiol fluorescent slides. The distance between adjacent spots, vertically and horizontally were measured and the percentage difference found between the distances produced using different slides. Each tissue grid (taken through different parts of the tissue, n=3) was compared pairwise to a plastic grid. Comparisons between mowiol and plastic were performed by averaging 3 grids for each and then comparing these averaged grids pairwise.

2.4 Data Analysis

ISM images were constructed from the simulated and experimental data using code written in Igor Pro 6.35 (WaveMetrics, Inc. Portland, Oregon, USA). Background image stacks collected with no laser excitation were subtracted from all experimental datasets prior to processing. Pixel reassignment and pinholing was performed based upon centre positions of either the detected emission maxima or applied excitation foci. The positions of detected emission maxima were determined using ThunderSTORM [14] an Image J plugin designed for single-molecule localisation or Localizer [15]. Excitation positions were read in directly from the

simulation code for the synthetic data, or generated from obtained reference grids using single-molecule localisation software for experimental data.

For each position, a sub-image centred on that position was extracted from the image. Sub-images were optionally pinholed around their centres by multiplication with a Gaussian function with a standard deviation of 2, 2.4 or 3.5 pixels depending on the data set. They were then expanded by a factor of two and placed into a canvas twice the size of the original image but centred on the same relative position. This process was performed for each position in each frame separately and all of the frames then summed to produce an ISM image. Corresponding mean projections (equivalent to a non-processed, summed projection but with reduced intensity) were produced from the original stack by finding the mean value of each pixel in every frame. Images were cropped and line profiles drawn along sections of interest. The full width half maximum (FWHM) values of individual actin filaments that crossed the line profiles were measured using the Gaussian fit function in Igor Pro to provide a quantitative comparison of the various processing methods used.

3. Results and discussion

3.1 Comparison of standard and non-standard ISM analysis schemes

Figure 5 compares the results of applying different image analysis schemes to a synthetic dataset for which the excitation positions are both accurately and precisely known. To evaluate the effects of standard and non-standard methods of processing ISM data, simulated data were generated from a test image (figures 5A and B "original") to provide a "ground truth" for comparison. The mean projection (figures 5A and B "Mean Proj") simulates normal widefield detection; this corresponds to convolving the original image with the excitation PSF and generates the lowest resolution image. Pixel reassignment around the known excitation coordinates (figures 5A and B "Pin Ex Scale Ex") is expected to give an improvement in resolution of √2 over widefield detection. FWHM measurements of stress fibres, presented in figure 5E are consistent with this. The mean FWHM of stress fibres in the mean projection image was 15.6 ± 1.2 pixels compared to 11.1 ± 0.8 pixels for the image created using pixel reassignment. Figures 5C and D show line profiles taken through a bundle of stress fibres to determine the typical contrast that can be achieved with each method. From the mean projection (red line) it is difficult to discern the three fibres present in the bundle. However, by applying pixel reassignment, the three peaks representing the three filaments present in the real image are regained. The practical improvement in resolution offered by pixel reassignment can be seen by comparing figure 6A mean projection, and figure 6B the reassigned image of a pollen grain taken using a multiphoton ISM instrument.

We then examined some non-standard variants on the scheme presented in figure 2 based on using the localised positions of the detected emission maxima as the axes for pinholing and/or scaling. Figure 5B (Pin Det Scale Ex) illustrates the images generated by using the locations of the detected maxima to centre the Gaussian function that is multiplied with the detected signal to simulate a macropinhole. Scaling is performed around the excitation axes as for standard pixel reassignment. By pinholing around the detected emission, the signal to background ratio of each subimage is maximized before the pixel reassignment stage. A line profile though figure 5B (Pin Det Scale Ex) is presented in figure 5D (blue) and shows an increase in feature contrast relative to the image generated by pinholing around the excitation focus (green). There is no significant change in feature size relative to images pinholed around the position of the excitation focus (figure 5E). Pinholing around the emission is of particular interest if there is reason to suppose that the reference excitation pattern is translated (discussed in section 3.2). An example of this approach applied to a real experimental dataset is presented in figure 6C.

In figure 5B the effect of pinholing and scaling around the detected intensity maxima is shown. The line profile (figure 5D, red) illustrates an increase in contrast while figure 5E indicates a slight reduction in measured feature size. The effects of processing experimental data in this way can be seen in on the pollen grain in figure 6D. These effects can be understood with reference to the differing positions of excitation foci and detected intensity maxima as a function of local fluorophore density shown in figure 3B. Scaling around the detected

intensity maxima effectively applies a local "gravitational" contraction, whereby the reassigned signal is drawn towards regions of high fluorophore density and the low intensity signals are suppressed, increasing the contrast at edges and making each individual stress fibre easier to detect. As this is an edge effect, the fractional reduction in size caused by scaling around the detected maxima is a function of feature size rising to ½ for point structures. Because the position of the detected maximum is specimen dependent, applying a contraction around these locations means that the final image is the result of spatially non-linear addition. Whilst scaling around the detection maximum causes a reduction in feature size compared with conventional pixel reassignment, the structure of the specimen is preserved and the edges intensified making this analysis option attractive for datasets where feature detection is desired, such as mapping networks or counting sub-resolution structures. If the excitation positions can be determined, it is preferable to scale around the excitation positions and then deconvolve using PSF_{eff} as this produces an undistorted image with the highest achievable resolution.

3.2 Displacement of reference grids

ISM image reconstruction requires knowledge of the excitation positions so that local contraction is performed around the optic axis. This is achieved by use of a reference grid obtained by performing an excitation scan on a uniformly fluorescing sample and extracting the coordinates. When the reference is accurate this is the preferred technique, but when there is a long time between images (creating potential drift) or the sample and specimen do not share a similar refractive index profile (e.g. a plastic reference slide for a hippocampal slice) then displacements can occur between the position of the excitation spots on the sample and on the specimen. Within our ISM system, displacements of reference excitation points by approximately one pixel (60 ± 30 nm) were observed when changing lateral position on a reference slide, or changing between reference slides, and approximately 5-6 pixels (320 ± 40 nm) of excitation drift over a five-hour period. If ISM was being used for a time-lapse experiment, the likely translation between the reference and true excitation co-ordinates would need to be taken into account.

Pixel reassignment using a translated reference excitation pattern serves only to translate the resulting image with no degradation in resolution. However when the technique is combined with the use of a digital pinhole to provide axial sectioning, the result is degraded. The effect of reference translation on pinholed ISM images is shown in figure 7A. As the displacement between the reference excitation coordinates used to process the data and the applied excitation PSF centres increases toward a maximum of 8 pixels tested here, a reduction in the signal to background ratio is observed (figure 7A). Displacement of the read-in coordinates by 4 pixels reduces the image intensity threefold (figure 7C). This is potentially ruinous for low signal specimens and an effect that could dramatically alter the relative intensity of the specimen over time.

The reduction in signal can be explained by considering the action of a digital macropinhole, which serves to multiply the detected signal by a Gaussian function. The act of rigidly displacing the excitation grid displaces the image obtained by that amount. When the centre of the pinhole is close to the centre of the detected emission maximum then very little light is lost, but if the detected maximum is displaced from the centre of the pinhole then the act of multiplication will cut out the majority of the detected light. If all of the pinholes are displaced from the detected maxima then every emission spot is reduced in intensity and the intensity of the final summed image is reduced.

We next examined whether it was possible to reclaim the signal to background ratio by pinholing around the detected intensity maximum before scaling around the excitation focus. In this way, the image intensity is maximised even for large displacements (figures 7B, D). The detection maxima are displaced from the emission maxima in a specimen dependent manner and this local displacement of the pinhole with respect to the excitation axis means that although the signal is increased the effect of the pinhole on the resulting summed image is no longer simply described by a convolution of a rectangular function with PSF_{em}. These different processing methods are illustrated with a real data set in figure 8. An alternative, global method of correcting

for grid translation was employed by York *et al. [7],* who determined the average offset of the excitation coordinates to the emission points before pinholing and scaling. The accuracy of this method is dependent on the number of detected maxima and may be affected by periodicity in the specimen itself.

3.3 Reference compatibility at depth

The previous section investigated the effect of a rigid body translation to the excitation coordinates, however other transformations to the excitation loci are possible. One of the major goals of optical microscopy is to image at depth within tissue. To determine the nature of any positional changes in the applied excitation loci when imaging at depth through tissue, we imaged a plastic fluorescent slide through 200 µm of fixed brain tissue. Analysis of the resulting grids revealed a 2 ± 2 % global scaling with respect to the reference positions on the fluorescent slide. We attribute this to the introduction of a layer of different refractive index. A similar, if smaller global scaling effect (0.6 ± 0.4 %) was observed between reference grids taken using plastic reference slides versus fluorescein mounted in mowiol under a coverslip. Changes in excitation grid size across the whole field of view under out experimental conditions are shown in figure 9 and represent a global scaling of excitation loci rather than a barrel distortion.

These results suggest that at increasing depth, the *in situ* excitation positions will be increasingly different from the standard reference positions recorded from the surface of a test slide. The displacement between the standard reference and the 'globally scaled' excitation loci that are actually applied to the specimen increases toward the periphery of the field of view resulting in a local loss of signal at the pinholing stage as described in section 3.2. A schematic diagram of this principle is shown in figure 9A. Using simulated data for which the ground truth is known, a 'vignetting' effect occurs (figure 9C). By pinholing around the detected maxima it is possible to restore the signal to noise ratio across the whole field of view (figure 9D). If high accuracy measurements are derived from ISM images at depth, globally scaling the reference with respect to the specimen results in an ISM image globally scaled by the same factor.

Whilst it is preferable to process the data using a reference slide with a refractive index profile closely matched to the specimen, this is not always possible and in practice it may be necessary to take a number of references and determine empirically which is the most compatible at the post-processing stage. Figure 10 shows the effect that processing the same experimental data with two alternative references has on real ISM datasets of tubulin in neuroblastoma cells. The difference in scaling between these two slides is insufficient to elicit a large change in intensity in this region of the image, but the impact that reference selection has on the line profile across a selection of tubulin is apparent. The relative differences in filament width may be a result of scaling between the two reference datasets or alternatively could be generated by variation in noise in the reference images and its subsequent effect on localization of the excitation foci. In either case, it is clear that it is advisable to take time to determine the most appropriate reference and ensure that results are robust to reference selection post-acquisition.

Conclusions

In this paper we considered the effect of standard and non-standard variants of pixel reassignment and digital pinholing on the images produced from ISM datasets. A test image was used to generate synthetic data from a simulated ISM microscope and provide a "ground truth". We used this synthetic data to confirm an improvement by a factor of 1.41 in the resolution of ISM images that have undergone pixel reassignment. We also investigated the effect of pinholing and scaling around combinations of excitation and detection maxima in both synthetic and experimental data. Single molecule localisation techniques can identify the position of detected emission peaks to very high precision and by applying a digital pinhole centred on these locations it is possible to retain signal from the image that would be otherwise lost (as in the case of displaced excitation points). Whilst scaling each sub-image around the detected emission maximum then summing does not create a true image of the sample plane, it does offer a helpful contrast enhancement in situations where the true excitation positions are unknown and standard pixel reassignment methods lead to a degraded image, such as

imaging at depth in tissue. Although computational rather than optical rescaling is an offline (and therefore slower) technique, only providing enhanced data after it has been taken, it does afford the opportunity to apply a variety of post-processing methods to explore the information content of an image.

Acknowledgements

We would like to thank the Biomedical Joint Workshops at the University of Leicester, Dr N. Moisoi and J. E. J. Adamson for assistance with cell culture and immunohistochemistry, Dr D. Pereda for supplying brain tissue, Dr J. T. Griffin for valuable discussions, Wellcome Images for supplying the test image and the BBSRC for funding this work (BB/L00691X/1; BB/L024284/1; BB/M012034/1).

References

[1] C.J.R. Sheppard, Optik, 80 (1988) 53–54.

[2] C.B. Muller, J. Enderlein, Physical review letters, 104 (2010) 198101.

[3] C.J. Sheppard, S.B. Mehta, R. Heintzmann, Opt Lett, 38 (2013) 2889-2892.

[4] A.G. York, P. Chandris, D.D. Nogare, J. Head, P. Wawrzusin, R.S. Fischer, A. Chitnis, H. Shroff, Nat Methods, 10 (2013) 1122-1126.

[5] P.W. Winter, A.G. York, D.D. Nogare, M. Ingaramo, R. Christensen, A. Chitnis, G.H. Patterson, H. Shroff, Optica, 1 (2014) 181-191.

[6] S. Roth, C. Sheppard, K. Wicker, R. Heintzmann, Optical Nanoscopy, 2 (2013) 5.

[7] A.G. York, S.H. Parekh, D. Dalle Nogare, R.S. Fischer, K. Temprine, M. Mione, A.B. Chitnis, C.A. Combs, H. Shroff, Nat Methods, 9 (2012) 749-754.

[8] O. Schulz, C. Pieper, M. Clever, J. Pfaff, A. Ruhlandt, R.H. Kehlenbach, F.S. Wouters, J. Grosshans, G. Bunt, J. Enderlein, Proc Natl Acad Sci U S A, 110 (2013) 21000-21005.

[9] I.J. Cox, C.J. Sheppard, T. Wilson, Applied optics, 21 (1982) 778-781.

[10] G.M. De Luca, R.M. Breedijk, R.A. Brandt, C.H. Zeelenberg, B.E. de Jong, W. Timmermans, L.N. Azar, R.A. Hoebe, S. Stallinga, E.M. Manders, Biomedical optics express, 4 (2013) 2644-2656.

[11] F. Ströhl, C. Kaminski, Methods and Applications in Fluorescence, 3 (2015).

[12] T. Wilson, Journal of microscopy, 244 (2011) 113-121.

[13] W.R. Zipfel, R.M. Williams, W.W. Webb, Nat.Biotechnol., 21 (2003) 1369-1377.

[14] M. Ovesny, P. Krizek, J. Borkovec, Z. Svindrych, G.M. Hagen, Bioinformatics, 30 (2014) 2389-2390.

[15] P. Dedecker, S. Duwe, R.K. Neely, J. Zhang, Journal of biomedical optics, 17 (2012) 126008.

Figure Legends

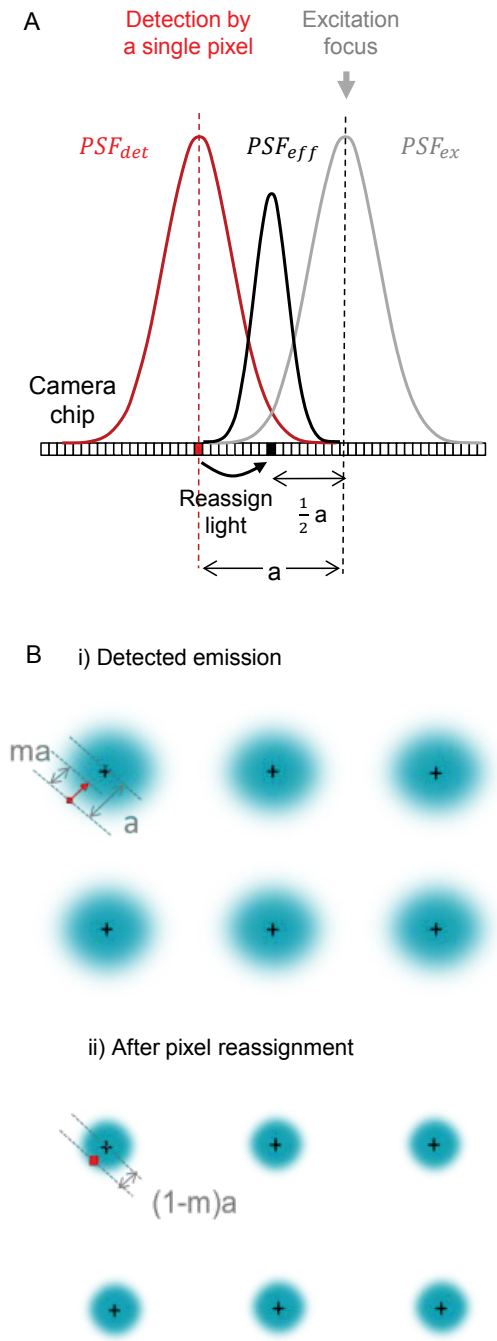

Figure 1. Schematic diagram illustrating the principles of pixel reassignment. A.) Shown is a 1D representation of the concept underlying pixel reassignment. The light detected by a single pixel (red) displaced by a distance 'a' from the excitation focus is most likely to have originated from the location of the peak of the product (PSF_{eff}) of PSF_{det}(x-a) and PSF_{ex}(x). In the case that PSF_{det} and PSF_{ex} are equal in width, (i.e. neglecting the Stokes shift) the maximum in PSF_{eff} occurs at a distance of a/2 from the excitation focus. The light from the pixel represented in red is thus reassigned to the position midway between the excitation and emission focus (black). For emission and excitation PSFs of differing widths, the scaling factor, m, is given by equation 1. In this representation m=1/2. B) Pixel reassignment in 2D: (i) a single image frame for a uniformly fluorescing sample showing emission generated by multiple excitation foci. (ii) After pixel reassignment, the image produced at each excitation focus appears locally contracted toward the excitation focus. Light detected at position 'a' is reassigned to a position (1-m)a from the excitation focus.

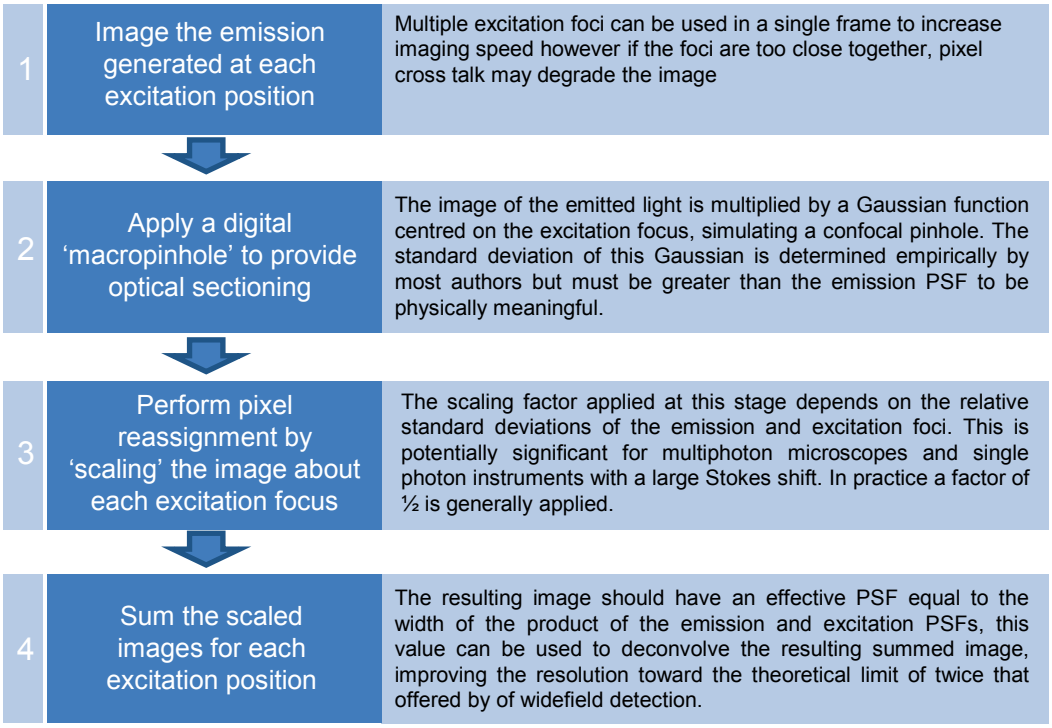

Figure 2. **Flowchart summarising the processes involved in image scanning microscopy**. Stages 2 and 3 can be performed optically or computationally. Any method of point scanning may be used to perform stage 1 but may have an impact on whether the emitted beam can be descanned such that optical methods of ISM image processing are possible. In standard pixel reassignment ISM, both pinholing and rescaling take place with respect to the excitation axis for each scan position.

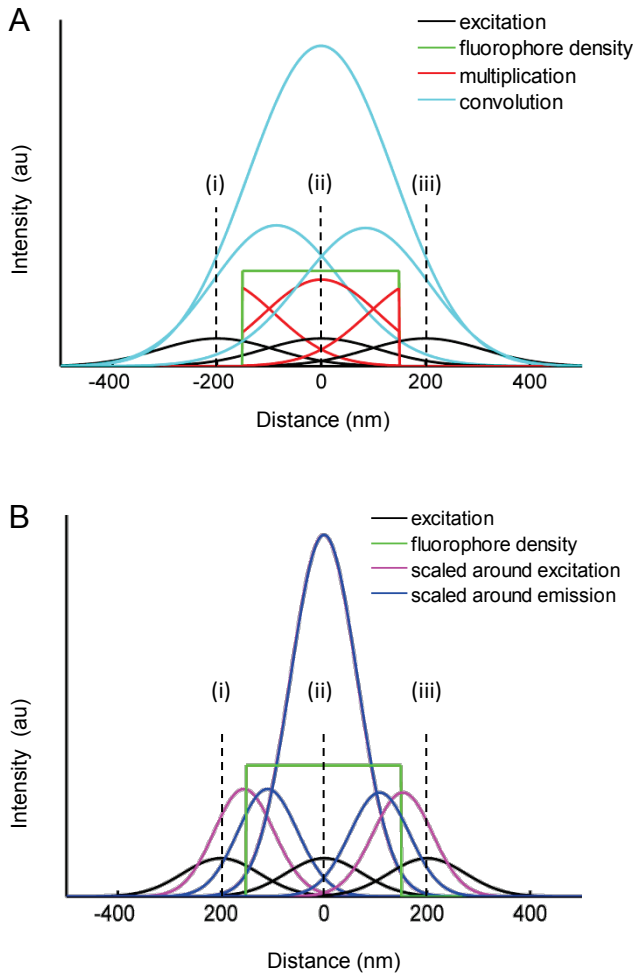

Figure 3. 1D simulation of image formation in ISM. A) A 300nm fluorescent object (green) is excited by three excitation foci (black) separated by 200nm. Excitation and detection wavelengths were the same (515 nm) for simplicity, corresponding to a theoretical FWHM of 187nm. The fluorescence generated from the sample is the product (red) of the fluorophore density and PSF_{ex}. This light is convolved with the emission PSF to simulate the signal detected by the pixels in the detection plane (cyan). If the specimen is excited centrally (excitation focus (ii)) the peak of the convolution is aligned to the excitation axis. As the excitation focus moves off this symmetrical location towards the edge of the fluorescent object the position of the detected maximum is increasingly drawn away from the excitation axis toward the specimen. Excitation positions (i) and (ii) are posited outside the specimen but still detect the signal which contributes to the final image when summed. At these positions the difference between the excitation and detection axes is clear. B) Excitation foci (black) and fluorescent object (green) are shown as per panel A. When performing pixel reassignment the detected signal is scaled around the excitation axis (magenta). Scaling around the detection axis draws the resulting signal (blue) toward the peak fluorophore density. Only at position (ii) do the signals coincide.

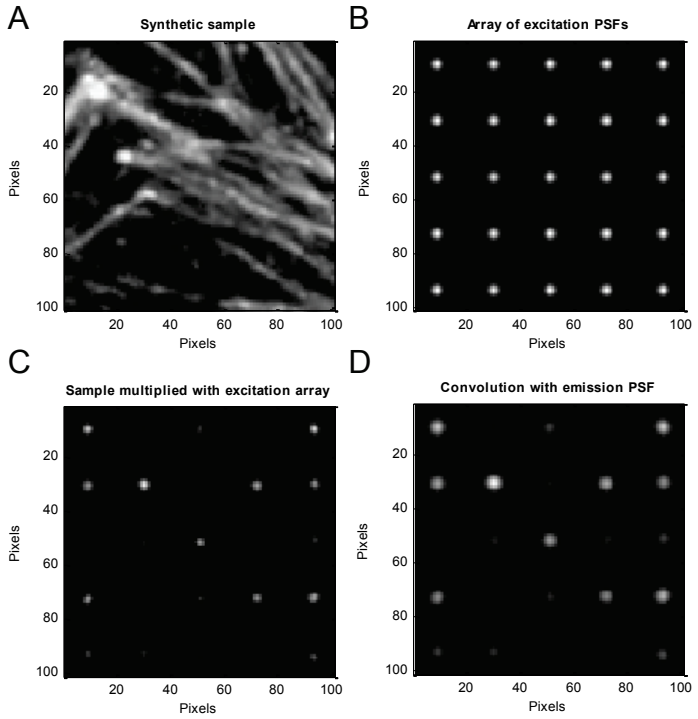

Figure 4. Schematic diagram of simulated ISM data creation. A) The sample image of actin stress fibres in a fibroblast cell was used as the basis for generating simulated ISM data. B) An array of theoretical excitation PSFs was used created to simulate a multifocal scan system. C) The sample image was multiplied by the PSF array. D) The multiplied image in C is convolved with the theoretical emission PSF. A cropped portion (100 x 100 pixels) of the full image (400 x 400 pixels) is shown for clarity.

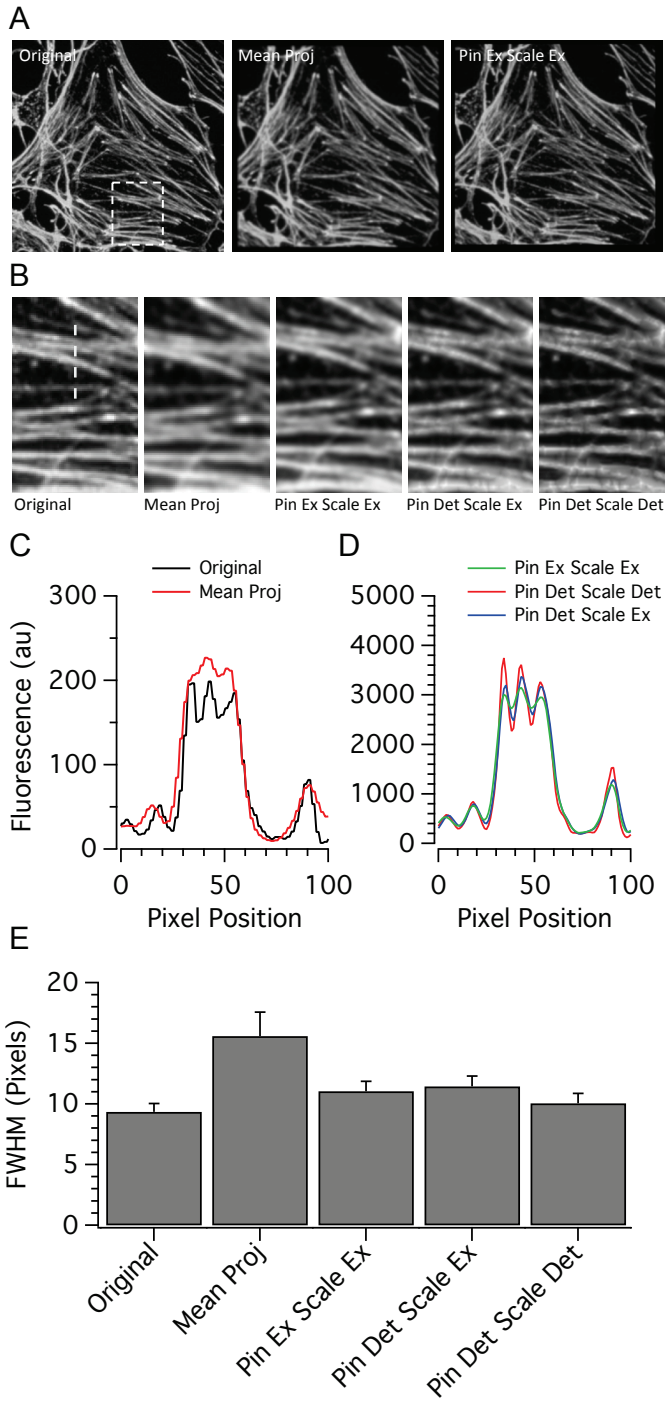

Figure 5. The effect of different data post-processing methods on simulated ISM data. A) Full sized images are shown of original, mean projection and ISM images. The ISM image was created by pinholing and scaling around the excitation coordinates. The mean projection simulates a widefield image convolved with the excitation PSF. B) Images cropped from the dotted region highlighted in panel A are shown to illustrate the actin fibre bundles in greater detail. Images are shown as in panel A with the addition of images that demonstrate the effect of pinholing around the detected emission and scaling around the known excitation and pinholing and scaling around the detected maxima. C) Line profiles through a bundle of three closely separated fibres (dotted line in panel B) for original and mean projection images are shown. D) Illustrates line profiles through the three pinholed and scaled images. E) FWHM values (mean ± SEM) for actin fibres for each of the post-processing techniques are shown (n=5).

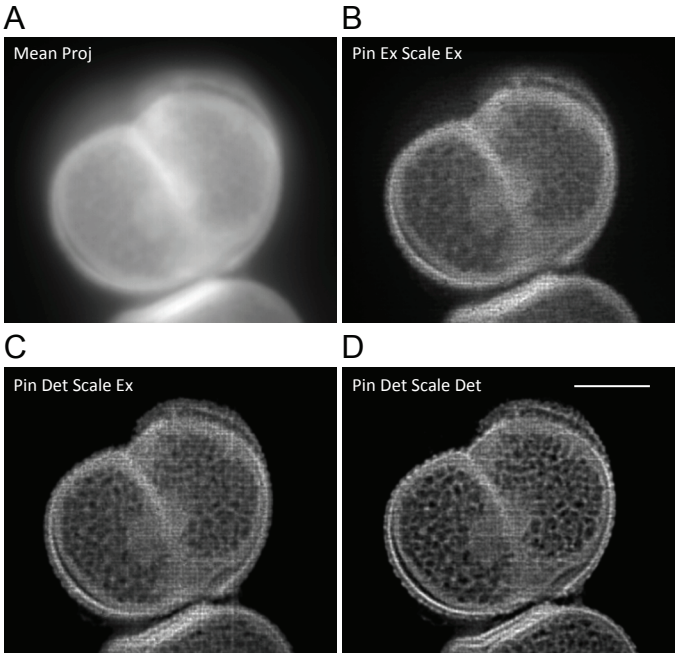

Figure 6: **The effect of different data post-processing methods on an experimental ISM data**. An autofluorescent pollen grain was excited at 780nm and image data collected with the multiphoton ISM instrument described in section 2.2. Data were processed using reference excitation loci derived from a plastic slide and a 'macropinhole' SD of 2.4 pixels. Images shown represent (A) the mean projection and data that were (B) pinholed and scaled around the excitation maxima, (C) pinholed around detected maxima then scaled around excitation maxima and (D) pinholed and scaled around detected maxima. The scale bar represents 10 µm.

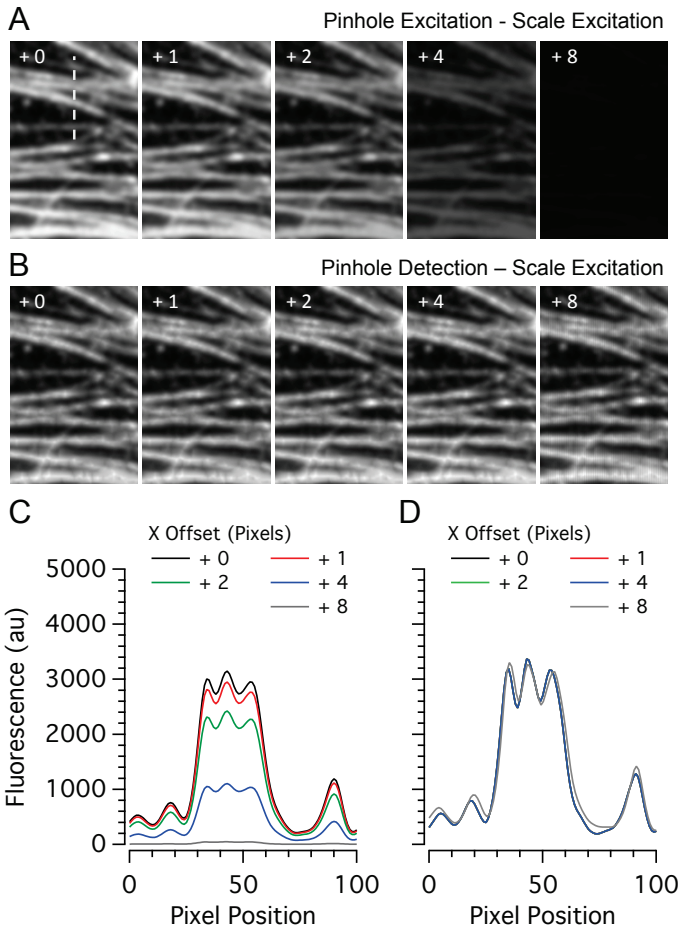

Figure 7. The effects of reference grid displacement in ISM images. A) ISM images from the same cropped region as in figure 4B are shown but with displaced excitation coordinates for pinholing and scaling. The numbers on the images indicate the extent of the displacement. Displacing the excitation coordinates relative to the applied excitation PSF causes a decrease in signal intensity in ISM images. B) Images created using displaced excitation coordinates to scale around but initially pinholing around detected maxima are illustrated. Here, the intensity is maintained at each pixel displacement. Panels C) and D) show line profiles of images from panels A) and B) respectively. In panel D, + 0 to + 2 pixel displacement profiles are plotted but are not visible because they are identical to the +4 (blue) profile. The +8 (grey) profile shows small deviations due to artefacts in the image formation process at large displacements.

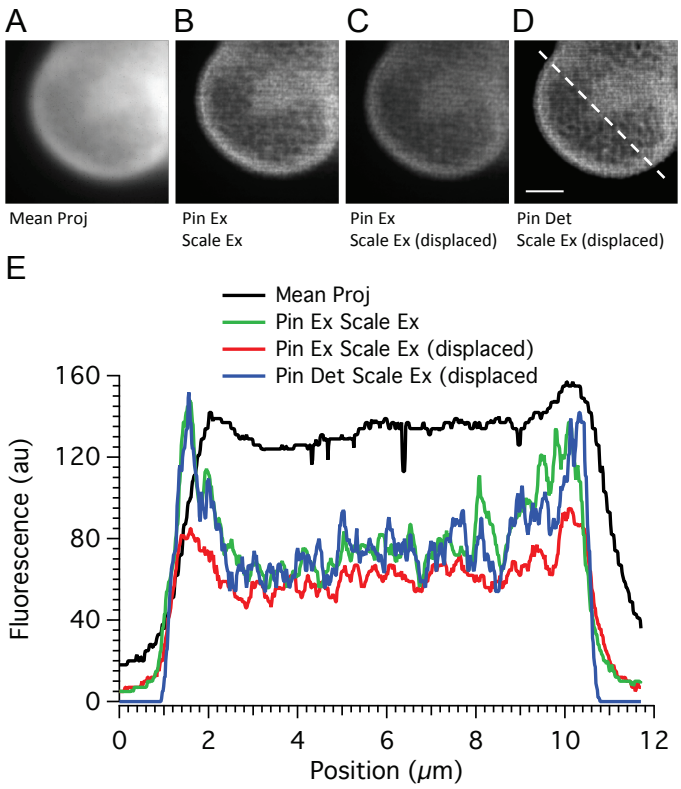

Figure 8: The impact of a translated excitation reference on ISM signal intensity. An autofluorescent pollen grain was imaged as described for Figure 6. Images shown represent (A) the mean intensity projection (B) an ISM image pinholed and scaled around appropriate reference excitation loci derived from a plastic reference slide using a macropinhole SD of 3 pixels. (C) illustrates an ISM image pinholed and scaled around reference excitation positions that were translated 4.5 pixels diagonally. The image in panel (D) was obtained by pinholing around the detected maxima and scaling around the translated reference positions. Panel (E) provides intensity profiles for each of the images (A-D) along the dotted line shown in (D). The scale bar represents 5 µm.

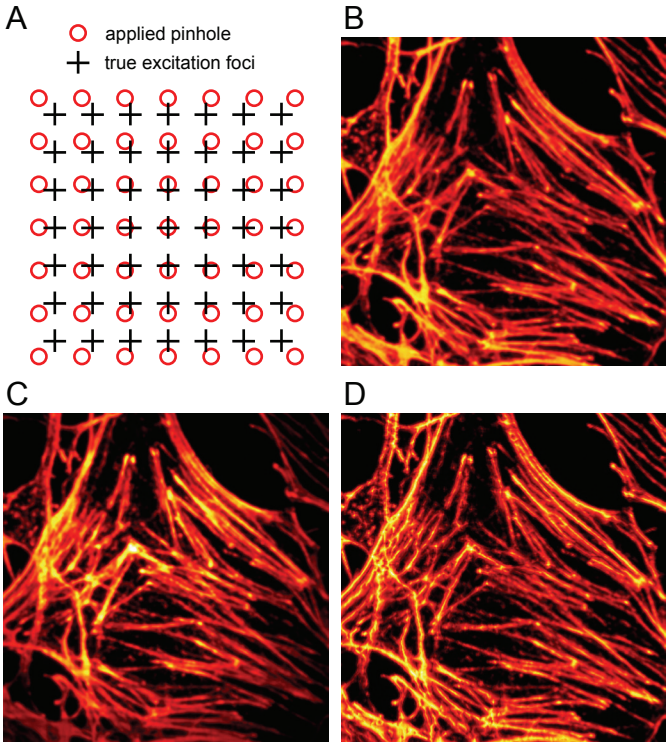

Figure 9: A simulated ISM dataset showing the impact of a 2% global scaling of the excitation foci relative to the applied reference excitation positions. (A) A schematic representation of global scaling of the true excitation foci (black crosses) relative to the applied pinhole positions derived from a standard reference (red circles). Not to scale. (B) A pseudocoloured ISM image pinholed and scaled around correct excitation positions. (C) An image resulting from pinholing and scaling around positions of a reference that was globally expanded by 2% relative to the correct excitation positions. Note the reduction in intensity around the periphery caused by a loss of signal at the pinholing stage. (D) An Image created by pinholing around the detected maxima and scaling around the globally scaled excitation reference positions. The loss of signal at the periphery of the image seen in (C) is restored. Lines introduced into images B and C by under sampling due to the global scaling were removed using a variant of the algorithm used by Winter *et al.,* 2014 [5]; relative intensities were kept constant by multiplying the resulting destriped image by a smoothed version of the summed intensity profile.

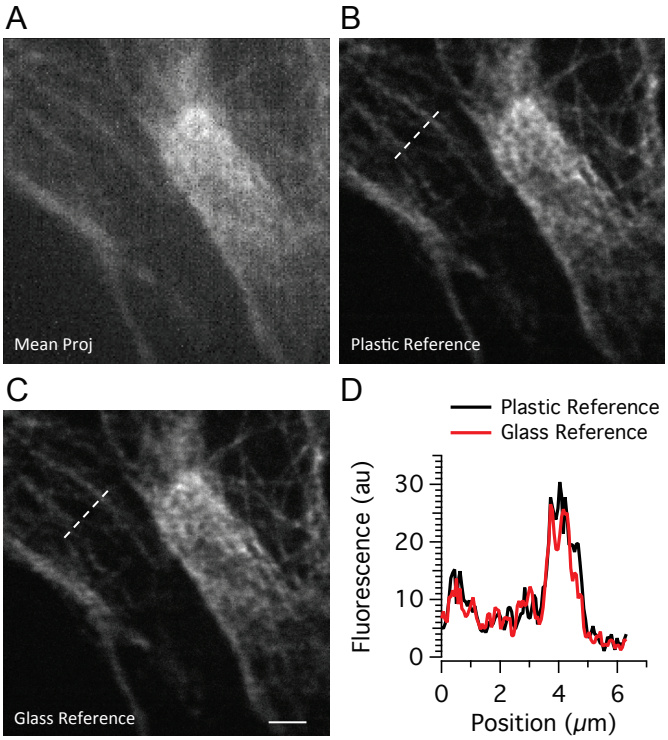

Figure 10: The impact of reference selection on ISM images of α-tubulin in cultured neuroblastoma cells . This dataset was collected using an excitation wavelength of 780 nm with the multiphoton ISM instrument described in section 2.2. Images shown are A) the mean projection (B) an ISM image pinholed and scaled around reference excitation foci determined using a plastic fluorescent slide, (C) an ISM image pinholed and scaled around reference excitation foci determined using a preparation of fluorescein and mowiol sandwiched between a coverslip and glass slide. (D) Intensity profiles through B (black) and C (red) are shown. Images B and C were destriped according to the protocol outlined in the legend to figure 9. The scale bar represents 5 µm.